Biophysical Chemistry 171 (2013) 54–62

Contents lists available at SciVerse ScienceDirect

Biophysical Chemistry

journal homepage: http://www.elsevier.com/locate/biophyschem

Probing the energetic and kinetic impact of topologically conserved interactions in the SIV gp41 six-helix bundle

Saša Bjelić [a,b,*], Ilian Jelesarov [a,**]

[a] Biochemisches Institut der Universität Zürich, Winterthurerstrasse 190, CH-8057 Zürich, Switzerland
[b] Case Center for Proteomics & Bioinformatics, CWRU School of Medicine, 10900 Euclid Road, Cleveland, OH 44106, United States

HIGHLIGHTS

- Transition state of immunodeficiency virus glycoprotein 41 exhibits compact native lake structure.
- Folding of the wild-type as well as most mutants can be described with simple monomer–trimer folding reaction mechanism.
- Formally the same mutations may have heavily different influence on transition state.

GRAPHICAL ABSTRACT

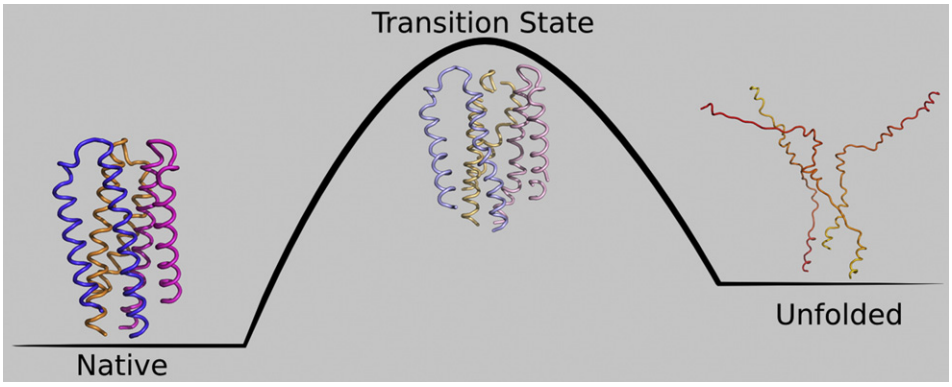

ARTICLE INFO

Article history:
Received 12 September 2012
Received in revised form 12 October 2012
Accepted 14 October 2012
Available online 23 October 2012

Keywords:
SIV gp41
Folding kinetics
Protein stability
Transition state

ABSTRACT

In this study we used an engineered six-helix bundle construct corresponding to the fusogenic core of the SIV gp41 protein as a model system to investigate the folding of a trimeric protein, which acquires a compact structure upon association of largely unstructured monomeric peptides. Thirteen mutants were generated in order to gain information about the thermodynamic and kinetic roles of topologically conserved tertiary interactions to folding and stability. The effect of the mutations was assessed by circular dichroism spectroscopy from urea-induced equilibrium unfolding experiments and in time-resolved mode to follow the kinetics of refolding and unfolding. While individual experiments can be interpreted in terms of a simple monomer–trimer refolding/unfolding reaction mechanism, comparison of equilibrium and kinetic data reveals that some variants clearly deviate from this two-state behavior and that most proteins cannot be classified as two-state folders without some reservations. Nevertheless, following "quasi-φ-value" and "quasi-β_I-value" analyses, we propose that the highest-energy barrier along the folding pathway is passed in the trimeric state, after the C-terminal half of each monomer chain is "fixed" in anti-parallel orientation to the surface of the central, still nascent N-terminal coiled-coil.

1. Introduction

The surface proteins of immunodeficiency viruses (HIV in humans, SIV in simians) play a key role in the early state of virus infection [1,2]. They are involved in docking of the virus to the cell surface and mediate direct fusion of the viral envelope with the cellular membrane. By

* Correspondence to: S. Bjelić, Case Center for Proteomics & Bioinformatics, CWRU School of Medicine, 10900 Euclid Road, Cleveland, OH 44106, United States. Tel.: +1 216 368 4784; fax: +1 216 368 6846.
** Corresponding author. Tel.: +41 44 635 5547; fax: +41 44 635 6805.
E-mail addresses: sasa.bjelic@case.edu (S. Bjelić), iljel@bioc.uzh.ch (I. Jelesarov).

0301-4622/$ – see front matter.
http://dx.doi.org/10.1016/j.bpc.2012.10.004

analogy with the structural changes in the influenza virus hemagglutinin (HA) protein, it has been postulated that a large-scale structural rearrangement of glycoprotein 41 (gp41) is involved in the transition of the metastable native (pre-fusogenic) state to a stable fusion-active (fusogenic) state [3,4]. The extracellular ectodomain of gp41 exhibits domain organization with several characteristic features which likely determine its role during activation of retroviral membrane fusion. This domain consists of an N-terminal glycine rich stretch, followed by two heptad repeats, separated by disulphide containing loop (Fig. 1). N-terminal hydrophobic, glycine-rich stretch (fusion peptide), is thought to insert into the cellular membrane at an early step in the fusion process [5]. The protein contains two regions with a 4,3 hydrophobic heptad repeat predicted to form coiled-coil structures [6,7]. The N-terminal heptad-repeat region is immediately C-terminal to the fusion peptide, while the C-terminal heptad-repeat region is located adjacent to the viral membrane. Between these two heptad-repeat regions is a loop region containing two cysteine residues.

At early stages of the membrane fusion process, the trimeric envelope glycoprotein spike contains gp41 in its pre-fusogenic conformation. Following binding to CD4 and its subsequent binding to the co-receptor CXCR5/CCR4, a transient gp41 species, the so-called pre-hairpin intermediate, is formed by exposure of the fusion-peptide region and concurrent formation of the N-terminal coiled-coil trimer [8–10]. The association of the C-terminal heptad-repeat region with the N-terminal coiled-coil resolves the pre-hairpin intermediate into the fusion-active hairpin structure and leads to apposition of viral and cellular membranes [11]. According to this model, the energy released by the formation of the trimer-of-hairpins is used to overcome the energy barrier associated with the energetically unfavorable fusion of the two lipid bilayers. In other words, refolding of gp41 into its fusogenic conformation and membrane fusion are mechanistically and thermodynamically coupled. Therefore, both the conformational stability of the trimer-of-hairpins and the rate of its formation play a critical role in driving membrane fusion. Indeed, there is evidence that destabilizing mutations within the six-helix bundle correlate with phenotypic changes [12,13].

Structural and biophysical studies have revealed that peptides corresponding to the N-terminal and C-terminal heptad repeats (N and C peptides), associate to form a stable, α-helical trimer of anti-parallel heterodimers [14,15]. Three N-helices form a central three-stranded coiled-coil, whereas the three C-helices pack in the reverse direction into highly conserved hydrophobic grooves around the outside of this coiled-coil [16–18] (see Fig. 1). It has been proposed that this structure likely represents the fusogenic state of gp41 [15,19]. Previous work from this laboratory has demonstrated that engineered constructs of the HIV and SIV gp41, which contain the characteristic features of the fusogenic state of gp41 (six-helix bundle; Fig. 1) are amenable to biophysical characterization. It has been shown that point mutations can have dramatic effects on the stability and folding/kinetics of gp41 [20,21]. The present work continues the efforts to understand the folding mechanism and the structural features determining the stability and dynamics of the gp41 trimer-of-hairpins. We employed mutational analysis to gain information on the gross structural properties of the folding transition state of the trimeric state of gp41, in which monomer association and folding are tightly coupled.

2. Materials and methods

2.1. Protein preparation and characterization

The construction of the expression vector, the expression and purification protocols of the SIV gp41 protein have been previously described [20,22]. Site directed mutagenesis was performed by standard

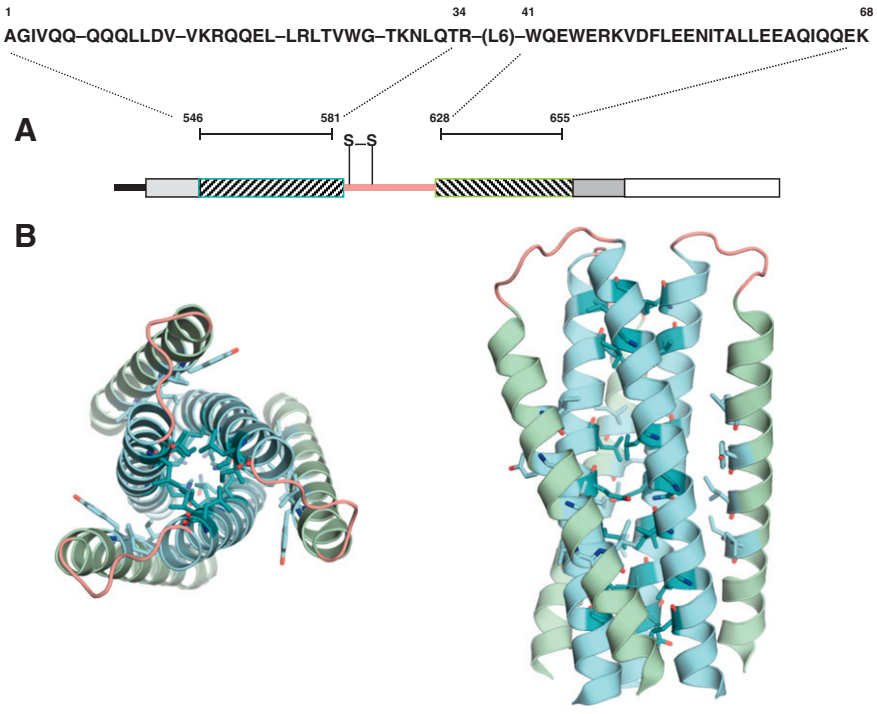

Fig. 1. Core structure of SIV gp41. A, Schematic view of the SIV gp41 ectodomain. The two hydrophobic heptad-repeat sequences are represented with hatched bars. The recombinant SIV model consists of the N34 and C28 peptides connected *via* a six-residue linker (L6 = SGGRGG) that replaces the disulfide-bonded loop region of gp41. The sequence of the SIV N34(L6)C28 model is shown. The sites of mutations are in bold. The dashes in the N-terminal half delineate the four heptad repeats. The residues are numbered 1 to 68; the correspondence to the sequential numbering of the SIV_{MAC} gp41 protein is indicated. B, Crystal structure of the six-helix bundle formed by the recombinant construct (pdb 1i5y). The left panel shows an axial view looking down the 3-fold axis of the six-helix bundle. The right panel shows a lateral view of the six-helix bundle. The N-terminal and C-terminal helices are colored in green and cyan, respectively. Mutated residues are depicted as sticks.

protocols using the Quick Change kit from Qiagen. The molecular mass of all protein variants was verified by mass spectrometry. Since no mutation involves replacement of an aromatic residue, protein concentration was determined under denaturing conditions (6 M GdmCl) using $\varepsilon_{280} = 17070\ M^{-1}\ cm^{-1}$ calculated from the amino acid sequence [23]. In the text, concentrations are given as monomer equivalents.

2.2. Buffer

All experiments were performed at 25 °C in PBS buffer (8.3 mM Na_2HPO_4, 1.47 mM KH_2PO_4, 137 mM NaCl, 2.7 mM KCl, pH 7.4, I = 164 mM). The pH of buffers containing urea was adjusted after addition of the denaturant. Urea concentrations were determined by measuring the refractive index.

2.3. Biophysical studies

2.3.1. Circular dichroism (CD) spectroscopy

Equilibrium unfolding experiments were performed on a Jasco-715 instrument (Jasco Ltd.), the calibration of which was routinely checked. In addition, for manual mixing kinetic experiments, models J-500 and J-810 were used. All spectrometers were equipped with a temperature-controlled water bath. Cylindrical jacketed cuvettes of 0.1 and 1.0 cm spectral paths were used. The samples were incubated overnight at 25 °C at the desired concentration of denaturant. The ellipticity at 222 nm was sampled for 3 min after complete thermal equilibration and averaged over 60 data points. Kinetic reversibility was checked by comparing the signals of samples prepared either from stock solutions without denaturant (native protein) or from stock solutions containing 8 M urea (unfolded protein).

2.3.2. Stopped-flow kinetics

Folding and unfolding experiments were performed with a π*-180 instrument (Applied Photophysics, Ltd.). Dead time was 1–2 ms; the optical path was 1 cm; the slits were set to 4 nm; the detection wavelength was 225 nm. Unfolding was triggered by rapid mixing of protein in PBS with buffer containing various concentrations of urea at a mixing ratio of 1:10 and a flow rate of 5 mL s^{-1}. Folding was initiated by mixing unfolded protein in 8 M urea with plain buffer or with buffered urea-containing solutions as to achieve the desired final denaturant concentration. The final protein concentration was 5–30 μM, and the final urea concentrations varied depending on the stability of particular variants. At least five kinetic traces were acquired and analyzed. Slow folding/unfolding was measured by manual mixing in a conventional CD apparatus. Dead time of these measurements was 10–20 s, negligible with respect to the half time of the reaction.

2.3.3. Analytical ultracentrifugation

Sedimentation equilibrium studies were performed on a Beckman XL-A analytical ultracentrifuge with an An-50-Ti rotor at 25 °C. Protein solutions were dialyzed overnight against PBS, loaded at initial concentration of 10 μM and analyzed at a rotor speed of 25000 rpm. Data sets (five per protein variant) were fitted simultaneously to a single-species model with the program NONLIN [24]. The protein partial specific volume and solvent density were calculated using SEDNTERP [25]. Molecular masses were all within 5% of those calculated for an ideal trimer. In no case systematic deviation from the statistical distribution of residuals was detected.

2.4. Data analysis

Primary analysis of equilibrium and kinetic data was performed according to simple two-state folding unfolding process involving only folded trimer (T) and unfolded monomer (M) using the formalism outlined in detail previously [20,21]. ϕ-values were calculated as:

$$\Phi = \frac{\ln k_f^{MUT} - \ln k_f^{WT}}{\ln K_{eq}^{WT} - \ln K_{eq}^{MUT}} \quad (1)$$

K_{eq}^{WT} and K_{eq}^{MUT} are the equilibrium unfolding constants of the wild type and the mutant proteins, respectively. In this case they are defined as $K_{eq} = \frac{k_f}{k_u} = \frac{[T]}{[M]^3}$, k_f and k_u being the folding and unfolding rate constants, respectively. Eq. (1) is generally valid for any solvent condition. To calculate ϕ in aqueous buffer, equilibrium and kinetic data collected in denaturant-containing solutions are extrapolated to obtain K_{eq} and k_f according to:

$$\ln K_{eq} = \ln K_{eq}(D) + \frac{m_{eq}}{RT}[D] \quad (2)$$

$$\ln k_f = \ln k_f(D) + m_f[D] \quad (3)$$

$K_{eq}(D)$ and $k_f(D)$ are the equilibrium constant and the folding rate constant at a given denaturant concentration, $[D]$. ($R = 8.314\ J\ K^{-1}\ mol^{-1}$ is the gas constant and T is the absolute temperature). The terms m_{eq} (in units of kJ $mol^{-1}\ M^{-1}$) and m_f (in units of M^{-1}) describe the dependence of the logarithm of the equilibrium constant and of the logarithm of the folding rate constant on $[D]$ in the general form $m = \frac{d\ln K}{d[D]}$. Likewise, the unfolding rate constant is calculated as:

$$\ln k_u = \ln k_u(D) + m_u[D] \quad (4)$$

3. Results

3.1. Experimental design

Prerequisites for a reliable mutational analysis of a protein can be summarized as follows. (i) The wild type and the investigated mutants thereof are not prone to aggregation in the concentration range suitable for biophysical experiments. (ii) The protein has appropriate thermodynamic stability to tolerate a set of non-disruptive point mutations. (iii) Spectroscopic signals report accurately and reproducibly the changes in the population of relevant molecular species in the course of time-resolved and equilibrium folding/unfolding transitions. (iv) Empirical (visual) or force field-based structural analysis suggests the existence of sites, where non-disruptive mutations can be introduced. Conditions (i), (iii), and (iv) pertain to both SIV-based and HIV-based constructs, as demonstrated previously [20,21]. We opted for the SIV protein (and not for a HIV-based construct) because SIV gp41 has higher solubility and better "in-solution" behavior [20,22]. However, the wild type protein (strain SIV_{MAC}), which we have previously characterized, is not particularly stable (mid-point of urea denaturation was 1.1 M with 5 μM protein [20], meaning that condition (ii) is not fulfilled. In order to avoid this problem and to be able to properly measure the folding kinetics in a wider concentration range of denaturants, we choose the T28I mutant as a pseudo-wild type, as its mid-point of urea denaturation is shifted by 2.9 M to higher urea concentration, in comparison to the genuine SIV_{MAC} wild type protein. (The correspondence between the numbering scheme used in this paper and the sequence of the SIV_{MAC} protein is shown in Fig. 1.) Like the genuine wild type, this mutation has been studied in great detail with respect to its thermodynamic [20] and kinetic [21] properties. The free energy obtained from equilibrium measurements is the same as that calculated from folding and unfolding kinetics. The m-value from equilibrium and kinetic experiments, m_{eq} and $m_{kin} = RT(lm_f l + lm_u l)$, respectively, are indistinguishable within error. Finally, the Tanford β-values (β_T) are reasonably close to each other (0.85 for wild-type, compared to 0.79 for pseudo wild-type), indicating that the T28I mutation does not significantly perturb the gross structure

of the transition state. For simplicity, we henceforth refer to the T28I pseudo-wild type as to WT.

The available X-ray and NMR 3D structures of SIV/HIV gp41 constructs reveal a conserved folding pattern. Our mutational strategy was the following: To probe the role of interactions stabilizing the internal three-stranded coiled coil we replaced all **a** and **d** positions of the four-heptad long 3, 4-repeat of the N-terminal helices with alanine. In the course of preliminary experiments, it was discovered that alanine is not tolerated at **d** position 24 (T24A) or **a** position 28 (I28A) and proper folding is prevented. These two mutants proteins were expressed in high yields, were soluble, yet no helical signal was observed at up to 200 μM concentration. To overcome this problem we designed two additional mutations T24I and I28T, guided by the observation that these positions are conservatively occupied by either threonine or isoleucine in naturally occurring SIV and HIV strains. Further, we replaced hydrophobic residues of the C-terminal helices by alanine. We targeted side chains that contribute to the hydrophobic core by making contacts exclusively with hydrophobic groups located in the internal coiled coil trimer. Altogether thirteen mutants were characterized. One class of mutants are "non-canonical" (polar *versus* non-polar side chains) whereas the rest create relatively large packing defects (Ile/Leu *versus* Ala). We consciously did not consider Ile/Leu → Val substitutions. It is well known that the strandedness of coiled coils critically depends on the nature of hydrophobic side chains in **a** and **d** positions [26,27]. Indeed, all mutant proteins are trimers as demonstrated by analytical ultracentrifugation (Fig. S1 and Table S1 in Supplementary material). On the other hand, in a parallel, in-register homotrimer, removal of even one methylene group would produce a large cavity in an **a** or **d** layer. Arguably, "non-canonical substitutions" violate the assumptions underlying the classical ϕ-value analysis and their effects are difficult to interpret. Nevertheless, the mutation sites are spread over the length of the protein and are potentially useful to understand the energetic and kinetic role of wild type interactions by "quasi-ϕ-value" and "quasi-β_T" analyses.

3.2. Equilibrium unfolding

The stability of all mutants was assessed from urea-induced unfolding at 25 °C. Fig. 2 shows examples of unfolding curves represented as the fraction of unfolded protein, f_U, as function of the denaturant concentration, [*D*] (see also Fig. S2 in Supplementary Material). As usual, f_U was calculated from the raw experimental traces ($[\theta]_{222}$ at various denaturant concentrations) assuming that the linear changes of $[\theta]_{222}$ at low and high urea concentrations represent the intrinsic ellipticity changes of the folded (trimeric) and unfolded (monomeric) ensembles, respectively. We noted that these pre-transitional and post-transitional $d[\theta]_{222}/d[D]$ functions for different mutants scatter significantly but did not detected any systematic trend (i.e. N-terminal versus C-terminal substitutions, or polar versus non-polar WT residues, or larger versus smaller WT residues). As seen in Fig. 2, within this approximation (the protein is fully folded at the onset of the unfolding transition (steep $d[\theta]_{222}/d[D]$ changes) and is fully unfolded after the unfolding transition), the unfolding curves exhibit no "steps" and are not unusually broad as to indicate the presence of intermediates differing in helical content. Following the (assumed) two-state model and the linear extrapolation model (LEM) the unfolding free energy changes in aqueous buffer, ΔG_{eq}, and the m_{eq} coefficients were calculated according to Eq. (2) and are listed in Table 1. With the exception of the Q7A variant, both ΔG_{eq} and $[D]_{1/2}$ values are lower than those measured for the WT protein, thus indicating significant destabilization effect of the corresponding mutations.

The scatter of the m_{eq}-values, 11.9 ± 1.7 kJ mol^{-1} M^{-1} (mean ± SD), exceeds the experimental error (δm_{eq} = 0.5 kJ mol^{-1} M^{-1}), but all m_{eq}-values are in agreement with statistical analysis of the protein database, which predicts an urea denaturation m_{eq}-value of 11.7 ± 0.9 kJ mol^{-1} M^{-1} for a protein consisting of 210 residues [28,29].

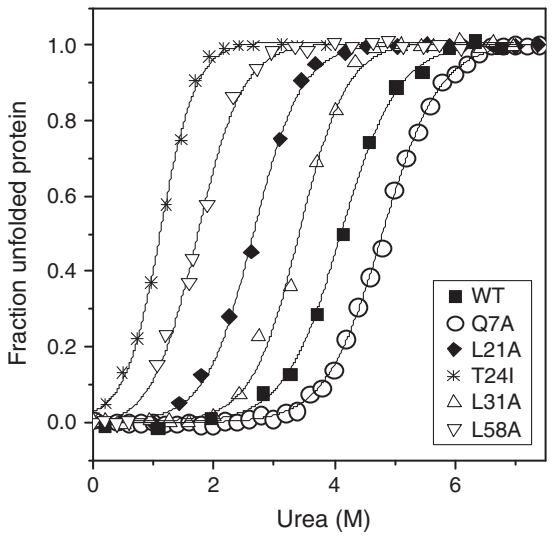

Fig. 2. Representative equilibrium urea-induced unfolding of SIV gp41 variants. The symbols represent the normalized CD signal ($[\theta]_{222}$) as function of the denaturant concentration. All experiments were performed at 25 °C in PBS, pH 7.0. Protein concentration was 5–30 μM. The symbol code is the following (curves left to right): T24I, asterisks; L58A, down triangles; L21A, diamonds; L31A triangles; WT, squares; Q7A, circles. The continuous lines are best fits according to a two-state model of unfolding and were calculated as described in ref. [20]. The unfolding curves of all variants can be found in Fig. S2.

Hence, the measured m_{eq} support the trimeric nature of all variants, the expected values being 7.9 kJ mol^{-1} M^{-1} and 15.5 kJ mol^{-1} M^{-1} for a dimer and a tetramer, respectively, and indicate, in general, low population(s) of possible monomer/dimer intermediates.

3.3. Folding/unfolding kinetics

Refolding and unfolding experiments were performed by following the time course of $[\theta]_{225}$ after rapid transfer of denatured protein to folding conditions or of native protein to denaturing conditions. Representative kinetic traces are shown in Fig. 3. As exemplified in Fig. 3, all collected traces can be perfectly described by numerical integration of the following equations, which describe the appearance or disappearance of the native trimer in refolding experiments or unfolding experiments, respectively:

$$\frac{dM}{dt} = -3k_f[M]^3 + 3k_u[T] \quad (5)$$

$$\frac{dT}{dt} = k_f[M]^3 - k_u[T] \quad (6)$$

The success of the analysis favors the simplest two-state kinetic model according to which only folded trimers and unfolded monomers are significantly populated along the reaction coordinate. As discussed previously [21,28], the presence of dimeric or trimeric intermediates cannot be excluded, yet they must be either very short-lived or spectroscopically "silent", i.e. they exhibit ellipticity signature which is indistinguishable within error from those of the folded and unfolded protein [28]. For further analysis we consider only kinetic experiments, which conform to the following requirements. First, the observed kinetic amplitude $\Delta MRE_{225} = MRE_{225,t=0} - MRE_{225,t=\infty}$ was at least 90% of the amplitude detected at equilibrium at each tested urea concentration. Second, the observed time window was shorter than 200 s to exclude baseline-drift artifacts (so far we have no evidence for slow folding phases. The protein contains no prolines which could introduce kinetic complications. Neither is there evidence

Table 1
Thermodynamic and kinetic parameters describing the stability and folding/unfolding of the SIV gp41 six-helix bundle.[a]

Variant	$[D]_{1/2}$ (M)	m_{eq} (kJ mol^{-1} M^{-1})	ΔG_{eq} (kJ mol^{-1})	ΔG_{kin} (kJ mol^{-1})	$k_f \times 10^{-12}$ (M^{-2} s^{-1})	$k_u \times 10^{3}$ (s^{-1})	$-m_f$ (M^{-1})	m_u (M^{-1})	m_{kin} (kJ mol^{-1} M^{-1})	β_T	φ_f
WT	**4.1**	**13.5**	**112**	**115**	**160**	**0.0011**	**3.8**	**1.0**	**11.9**	**0.79**	**–**
Q7A	4.8	11.0	111	94	180	2.5	2.7	0.4	7.6	(0.88)	N.D.[b]
L10A	**2.8**	**10.6**	**89**	**86**	**1.3**	**1.2**	**3.3**	**0.8**	**10.2**	**0.80**	**0.51**
V14A	**3.2**	**11.8**	**96**	**94**	**1.7**	**0.048**	**2.7**	**0.8**	**8.7**	**0.78**	**0.69**
Q17A	**3.5**	**10.4**	**95**	**95**	**140**	**2.9**	**2.0**	**1.2**	**7.9**	**0.62**	**0.02**
L21A	2.7	13.1	91	78	0.14	3.7	3.5	0.4	9.4	(0.91)	(0.82)
T24I	4.0	12.9	111	91	5.6	0.54	2.1	1.1	7.8	(0.66)	(1.50)
I28A	**1.1**	**16.1**	**75**	**76**	**0.12**	**5.8**	**5.5**	**1.3**	**16.8**	**0.81**	**0.48**
L31A	**3.4**	**12.6**	**102**	**95**	**6.1**	**0.14**	**2.8**	**1.3**	**10.2**	**0.69**	**0.80**
V48A	**2.8**	**14.3**	**98**	**97**	**2.3**	**0.021**	**2.7**	**1.3**	**10.1**	**0.67**	**0.73**
I51A	**3.1**	**9.6**	**88**	**94**	**5.2**	**0.16**	**4.3**	**1.0**	**13.2**	**0.81**	**0.36**
I55A	**2.0**	**11.0**	**83**	**91**	**0.49**	**0.062**	**2.5**	**1.5**	**9.9**	**0.62**	**0.50**
L58A	1.7	14.0	77	114	320	0.0036	5.1	1.3	15.8	(0.79)	(−0.05)
L59A	3.5	12.5	104	80	14	140	4.1	1.0	12.7	(0.81)	(0.71)

[a] All experiments were performed at 25 °C in PBS, pH 7.4. Protein concentration was 5–30 μM (monomer). In bold: mutations obeying a relaxed two-state criterion. The estimated errors of equilibrium parameters are: 0.1 M in $[D]_{1/2}$; 7–10 kJ mol^{-1} in ΔG_{eq}; 0.5 kJ K^{-1} mol^{-1} in m_{eq}. Individual kinetic constants were determined with precision always better than 5% from repeated experiments. The principal errors of k_f and k_u listed in the Table are due to the extrapolation to zero denaturant. They were estimated from the confidence bands (0.95 level) calculated by regression analysis. Since the extrapolation of k_f is short, the mean error in k_f is 4%. The extrapolation errors in k_u range from 5% to 30%. The precision of m_f and m_u is within 0.1 M^{-1}, as estimated by jack knife analysis. The errors in φ_f are in the order of 20% from propagation of errors in ΔG_{eq} and k_f. Entries in bold correspond to variants, which obey the $0 < |\Delta G_{eq} - \Delta G_{kin}| < 10$ kJ mol^{-1} criterion.

[b] Not determined as $\Delta\Delta G_{eq}^{WT\text{-}Q7A}$ is virtually indistinguishable.

for formation of burst-phase helical intermediates). These two conditions somewhat reduce the range of urea concentrations at which folding/unfolding kinetics was subjected to analysis, but provide a rigorous basis for analysis of the major folding/unfolding event (it is *a priori* clear that minor conformational changes are not observable by CD).

Following linear extrapolation method (LEM), the microscopic rate constants, k_f and k_u, were calculated by extrapolation of the $\ln k_f$ or $\ln k_u$ *versus* $[D]$ functions to $[D] = 0$ according to Eqs. (3) and (4). Examples of Chevron plots, which are all linear in the studied range of urea concentrations, are shown in Fig. 4 (see also Fig. S3 and S4 in Supplementary material). The derived rate constants are listed in Table 1 along with the corresponding m_f and m_u coefficients.

4. Discussion

4.1. Energetic and kinetic properties of some variant gp41 constructs

A comprehensive discussion of the consequences of mutating all wild type side chains is not possible in the absence of high-resolution structural information for each construct. Nonetheless, the effects of some of these mutations are worth commenting on. In view of the fact that the mutations generally destabilize the wild type six-helix bundle, the energetic neutrality of the Q7A and T24I substitutions is intriguing (ΔG_{eq} in Table 1). In both cases a polar interaction is eliminated. Comparison with the highly destabilizing I28T mutation (which is the most destabilizing in the set!) and the modestly destabilizing Q17A

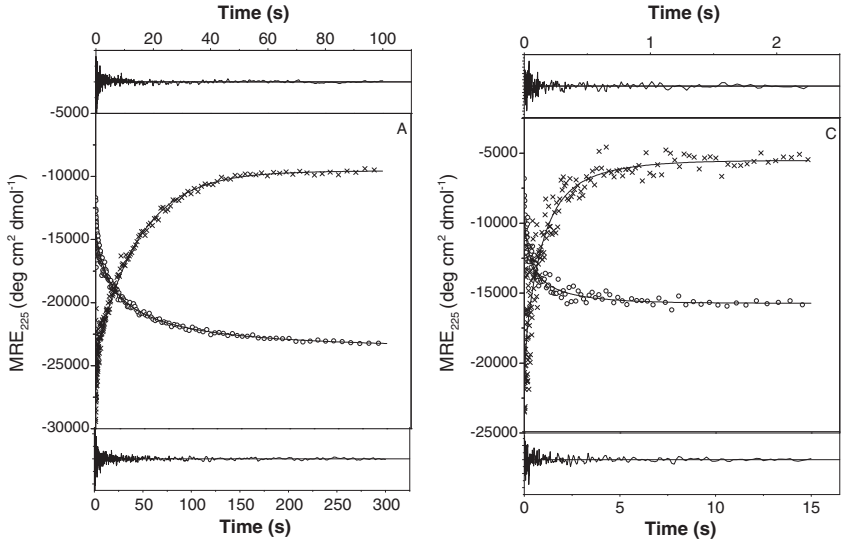

Fig. 3. Representative stopped flow experiments with SIV gp41 variants. Folding and unfolding traces are shown with circles and crosses, respectively. The continuous lines were calculated by numerical integration of Eqs. (5) and (6). The deviations of the calculated functions from the experimental data are shown in the top (unfolding) and bottom (folding) panels. The time scales of the folding experiments and unfolding experiments are on the lower *x*-axis and upper *x*-axis, respectively. Panel A, Results with L10A: folding in 1.5 M urea (12.3 μM protein) and unfolding in 4.8 M urea (6.8 μM protein). Panel B, Results with L59A: folding in 1.9 M urea (10.9 μM protein) and unfolding in 2.6 M urea (6.3 μM protein). The observed CD-signal fits well with equilibrium one, indicating not additional slow phase. All experiments were performed in PBS at 25 °C.

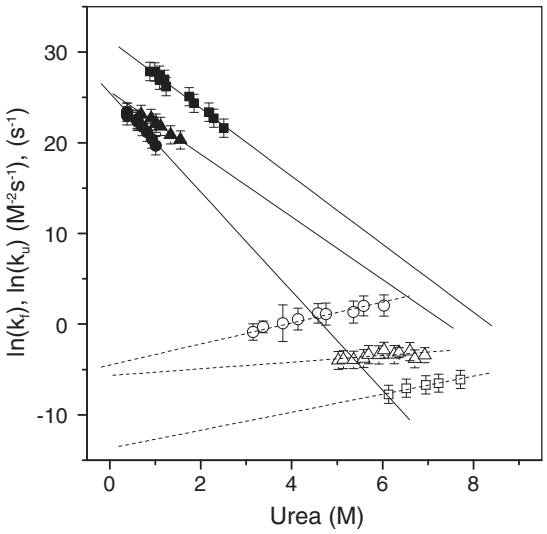

Fig. 4. Representative chevron plots constructed for SIV gp41 variants. Filled symbols and continuous lines, folding data. Open symbols and dashed lines, unfolding data. Squares, wild type protein; circles, I28T; triangles; L21A. See Fig. S3 for all variants.

mutation reveals that in the formally identical **a** positions of the first and fourth heptad (7 and 28, respectively) non-polar interactions confer stability, while in the **d** positions of the second and third heptad (17 and 24, respectively) polar interactions are important.

This energetic non-equivalence of **a** and **d** positions in coiled coils has been previously demonstrated [30,31]. Hydrophobic side chains residing in the middle of the central coiled coil (L10, V14, L21) stabilize the trimer to approximately the same extent. Differently, there is a clear trend that mutations that disrupt the interactions linking the C-terminal helices to the central coiled coil by hydrophobic contacts are more destabilizing the closer the corresponding sites are to the middle of the six-helix bundle (compare the increasing effect of V48A, L51A, I55A and L58A). More surprising is the fact that the L59A is one of the least destabilizing mutations. Simple structural analysis (of highly related X-ray structures of SIV and HIV constructs) rationalizes the large difference between the L58A and L59A mutations by the fact that, although both side chains are completely buried, the hydrophobic packing is much more optimized for L58 than for L59. This is only a tentative explanation since both L58A and L59A show the largest deviations from the 2-state model (see below). Excluding L59A, among the conservative hydrophobic-to-alanine mutations, variants L31A and V48A have the smallest effect on stability. This probably reflects the fact that these two sites are closest to the loop region and experience larger structural fluctuations (less well optimized hydrophobic complementarity) than the rest of the probed sites.

Most of the mutants fold slower and unfold faster than the WT protein (Table 1 and Fig. S5 in Supplementary material). In terms of folding rates, mutations Q7A, Q17 and L58A are kinetically inert, their relative folding rates, $k_{f,rel}=k_f^{MUT}/k_f^{WT}$ being between 0.5 and 2. For five mutants, V14A, T24I, L31A, V48A, I51A, and L59A, $k_{f,rel}>0.01$. Slowest folding ($k_{f,rel}<0.01$) show variants L10A, L21A, I28T, and I55A. In terms of unfolding, *all* variants are destabilized. The relative unfolding rates, $k_{u,rel}=k_u^{MUT}/k_u^{WT}$, rank the mutations in three (also arbitrarily defined) categories: (i) barely destabilized ($10<k_{u,rel}<100$; V14A, V48A, I55A), (ii) modestly destabilized ($100<^{ku,rel}<1000$; T24I, L31A, I51A), and (iii) highly destabilized ($k_{u,rel}>1000$; Q7A, L10A, Q17A, L21A, I28A). The clear exceptions are variants L58A ($k_{u,rel}<5$) and L59A ($k_{u,rel}>1\times10^5$). The former unfolds like the WT protein; the latter unfolds dramatically faster. As already mentioned, and as it will be discussed below, the assumptions implicit in the two-state model are not met by these variants, thus making it difficult to rationalize such a tremendous difference in kinetic stability caused by formally identical mutations. However, we note that these sequentially adjacent side chains make hydrophobic links to different inner helices. As a tentative explanation, we suggest that the L58A/L59A "hydrophobic fork" located approximately half way from the ends of the six-helix bundle is a hot spot in stabilizing the native state, the hydrophobic packing of L59 being less well optimized (see above). Removal of three methylene groups by mutation to alanine introduces a packing defect. In this particular site, the loss of hydrophobic interactions involving L59 cannot be compensated by neighboring interactions, and, as the consequence, thermal fluctuations overcome some critical threshold. As seen in Fig. 7, the apparent φ-values of L58 and L59 are very low and rather high, respectively. Notwithstanding all reservations in interpreting this difference (both variants are non-two-state folders), the interactions made by L59 appear to be crucial for proper folding.

The changes in the folding and unfolding rates caused by non-canonical polar-*versus*-nonpolar substitutions also deserve attention. It appears that glutamine-to-alanine mutations are balanced in a similar way by compensating changes (decrease) in k_f and k_u. In heptads 1 and 4 of the N-terminal coiled coil, nonpolar side chains in **a** positions appear to speed up folding more than they slow down unfolding (compare the changes in k_f and k_u of Q7A and I28T relative to WT). In contrast, polar side chains in positions **d** of heptades 2 and 3 are beneficial in terms of both folding and unfolding, in agreement with the conclusions drawn from analysis of ΔG_{eq} (see above).

4.2. Two-state versus non two-state folding/unfolding mechanism

In the framework of "classical" mutational (φ-value) analysis of the folding/unfolding mechanism, the definition of criteria ruling the acceptance or rejection of the two-state approximation is a crucial step. It is clear that equilibrium, quasi-sigmoidal unfolding curves, kinetic, quasi-exponential traces, in the absence of abrupt signal changes and linear chevron plots, can be formally discussed as describing a two-state process. A stronger criterion is the comparison of the free energy changes derived from equilibrium and kinetic experiments, $\Delta G_{eq}=-RT\ln K_{eq}$ and $\Delta G_{kin}=-RT\ln K_{kin}=k_f/k_u$, respectively [32]. Fig. 5 illustrates that ΔG_{eq} and ΔG_{kin} are not correlated ($R^2=0.04$), in sharp contrast to the definition of two-state behavior. However, the experimental uncertainties should be considered. We conservatively estimate the mean ΔG error in the set as being 7–10 kJ mol^{-1}. According to this criterion, nine proteins can be classified as two-state folders (WT, L10A, V14A, Q17A, I28T, L31A, V48A, I51A, and I55A). The ΔG_{kin}-*versus*-ΔG_{eq} correlation coefficient for these proteins is $R^2=0.951$ (Fig. 5).

Another test for the fulfillment of the two-state mechanism is the comparison of the Brønsted coefficients for the folding and unfolding reactions [33]. The Brønsted coefficient is defined in the following way:

$$\beta=\frac{d\ln k}{d\ln K} \tag{7}$$

where k is a rate constant and K is the genuine equilibrium constant (derived from experiment(s) performed at equilibrium conditions, and not derived from the k_u/k_f ratio). In protein folding, the two-state model is valid if the Brønsted coefficient for the folding and unfolding reactions, β_f and β_u, respectively, add up to unity, i.e.:

$$|\beta_f|+|\beta_u|=1 \tag{8}$$

In the studied set of mutations, both β_f and β_u are close to zero (Fig. 6). However, for proteins that have been selected as two-state folders, based on the ΔG_{kin}-*versus*-ΔG_{eq} correlation, $|\beta_f|+|\beta_u|=0.9\pm0.2$.

Finally, we examine the correspondence between the m_{eq} and $m_{kin}=RT(|m_f|+|m_f|)$ coefficients as a test for the validity of the two-state model. For a two-state transition, $m_{eq}=m_{kin}$ within error.

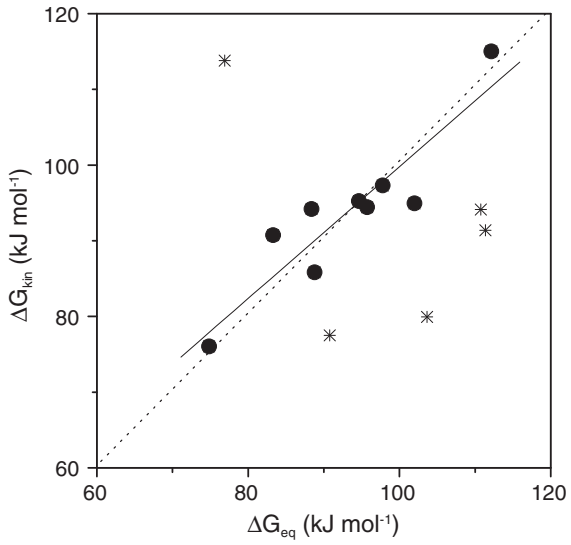

Fig. 5. Correlation between the unfolding free energy changes obtained from equilibrium (ΔG_{eq}) and kinetic (ΔG_{kin}) experiments. ΔGs were calculated assuming a two-state model of folding/unfolding ($\Delta G_{eq} = -RT\ln K_{eq}$; $\Delta G_{kin} = -RT\ln(k_u/k_f)$). The squares represent data fitting the following criterion: $0 < |\Delta G_{eq} - \Delta G_{kin}| < 10$ kJ mol^{-1}. The solid line is the correlation line describing these data only ($R^2 = 0.951$). The dashed line represents the ideal expected correlation ($R^2 = 1$).

The two sets of m-values do not differ statistically ($m_{eq} = 11.9 \pm 1.7$ and $m_{kin} = 10.9 \pm 2.8$ kJ mol^{-1} M^{-1}; mean ± SD). However, all but three mutations(L10A, I55A, and L59A), exhibit $m_{eq} - m_{kin}$ differences larger than the estimated experimental error. (Note that the L59A protein doesn't fit the ΔG_{kin}-*versus*-ΔG_{eq} criterion as a two-state folder). On a closer look, the difference between m_{eq} and m_{kin} stems from a larger variation in m_f (Table 1). Furthermore, there are no cross-correlations between m_{eq} and m_{kin} to ΔG_{eq} and ΔG_{kin} (in absolute values and in relative changes). The reason for this discrepancy is not known.

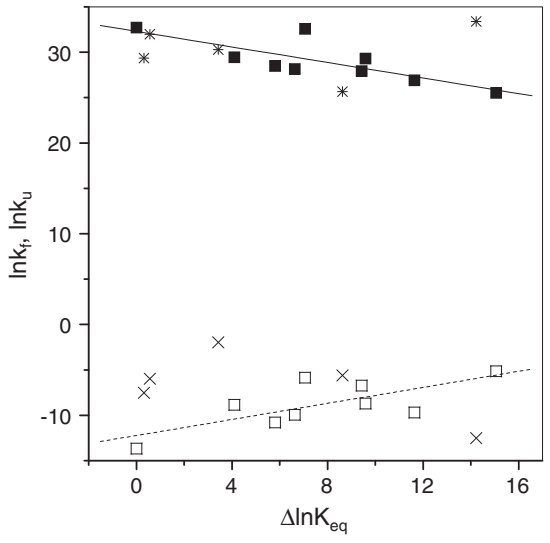

Fig. 6. Brønsted plot for folding and unfolding of the SIV gp41 six helix bundle. The solid symbols and asterisks represent the complete set of lnk_f data. Likewise, the open symbols and crosses represent the complete set of lnk_u data. $\Delta\ln K_{eq} = \ln(K^{MUT}/K^{WT})$ is the change of the unfolding constant calculated from equilibrium data. The squares highlight lnk_f (solid) and lnk_u for proteins pertaining to the criterion: $0 < |\Delta G_{eq} - \Delta G_{kin}| < 10$ kJ mol^{-1}. The lines are the correlation functions to the folding and unfolding data considering only these variants (continuous and dashed, respectively). The values of | slope | = dlnk/dlnK_{eq} representing the Brønsted coefficients are 0.45 ± 0.13 (folding) and 0.44 ± 0.16 (unfolding).

Previously, the WT, T24I and I28T [20], as well as two HIV gp41 proteins [33] have been classified as two-state folders based on equilibrium information only (analysis of calorimetric experiments and comparisons between thermal and isothermal unfolding data). The kinetic data collected in this work add a further level of analysis and demonstrate that some variants clearly deviate from the two-state behavior and most proteins cannot be classified as two-state folders without some caveats. Nevertheless, in view of the experimental errors, nine proteins fold/unfold with a reasonable resemblance to a two-state process, as to provide hints about the gross structure of the transition state.

4.3. Properties of the transition state

The structure of the rate-defining, high-energy state, which proteins transverse on the folding/unfolding coordinate, has attracted considerable attention in recent years, because it provides important clues about the sequence of structural events along the folding/unfolding pathway i.e. of the folding/unfolding mechanism. The identification of the set of interactions realized in the transition state is only possible by site directed mutational analysis in the framework of the φ-value [32,34]. This methodology has been extensively used in studies of small monomeric proteins [35–37], and only occasionally in studies of oligomeric proteins [38], including short coiled coil dimers [39]. To our knowledge, φ-value analysis has never been performed with a trimeric protein, where the association of (largely) unstructured monomers and folding to the native trimer is concurrent processes. In contrast to monomeric proteins, it cannot be *a priori* excluded that the passage of the rate limiting step in folding of an oligomeric protein is sensitive to the total protein concentration due to population of concentration-dependent intermediate states [28]. In the limited concentration range of our experiments (5–30 μM) we did not observe any concentration dependence of the rates of folding (and unfolding).

Fig. 7 shows the φ-values calculated according to Eq. (1). In the set of "quasi-two-state" folders, L10A, I28T, I51A, and I55A exhibit $\varphi < 0.5$. For three mutants, V14A, L31A, and I55A, $\varphi > 0.5$. In the usual interpretation, partial φ-values (between 0.3 and 0.7) are difficult to interpret [36]. Such φ-values indicate either partial formation of native-like interactions involving the WT side chain in conformationally homogeneous TS, or the existence of alternative local conformations within the transition state (TS) ensemble, or even the existence of largely different transition states (parallel folding pathways). The clear "outlier" is Q17A showing a negligibly small φ. However, we consider this φ-value as being artificial, since both ΔG_{eq} and k_f are indistinguishably close to the wild type parameters. For these reasons we are reluctant to discuss the meaning of individual φ-values in terms of local structure. The quasi-φ-values collected in this study are clearly of low-resolution, or of "weak" informational content [40]. Nonetheless, the following points are worth noting: (i) The mean measured φ is 0.50 ± 0.25. (ii) The mutations cover three quarters of the length of the elongated six-helix bundle. (iii) Similar φ's were calculated for sites close to the N-terminus (L10, V14) and to the C-terminus (I28) of the central coiled coil. (iv) Similar φ's were calculated for side chains participating in the hydrophobic core of the internal coiled coil and side chains linking (by hydrophobic packing) the outer C-terminal helices to the inner N-terminal helices. (v) The φ-values for L31 from the N-terminal helix and V48 from the C-terminal helix are not significantly different. These two side chains are sequentially positioned up-stream and down-stream of the loop region. All these observations strongly suggest that the transition state is compact and the outer and inner helices are oriented in a native-like fashion (anti-parallel). Based on the available information, TS can be defined as being "diffuse" in the sense that there is no obvious polarity in the distribution of φ-values. These conclusions are further supported considering the apparent φ-values for non-two-state mutants (Fig. 7).

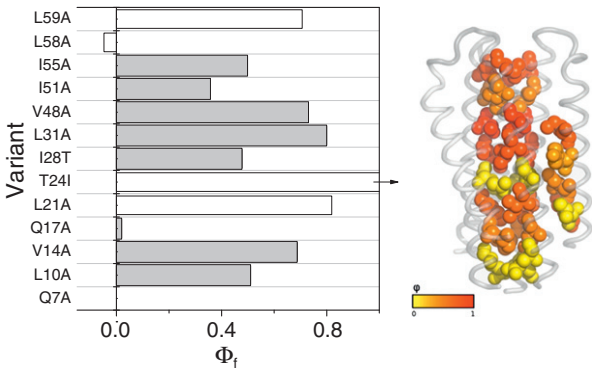

Fig. 7. φ-values characterizing mutations of the SIV gp41 six-helix bundle core. Left panel: φ-values were calculated by Eq. (1). The shaded bars represent φ-values for mutations which obey quasi-two state behavior (based on the $0<|\ \Delta G_{eq}-\Delta G_{kin}\ |<10$ kJ mol^{-1} criterion). The arrows indicate $\varphi>1$. Right panel: color-coded distribution of φ-values in the 3-D structure of gp41. The yellow and red colors represent φ-value of 0 and 1, respectively. For clarity, only one C-terminal helix is decorated with side chains. The numerical values are listed in Table 1.

The compactness and the diffuse character of TS can also be inferred from the calculated Tanford's β-value. This dimensionless parameter in the two-state approximation is defined as [32]:

$$\beta_T = \frac{|m_f|}{|m_f| + |m_u|} = 1 - \frac{|m_u|}{|m_f| + |m_u|} \quad (9)$$

The numerical value of β_T ($0<\beta_T<1$) is usually interpreted as an indicator of the position of TS on a reaction coordinate in terms of denaturant-sensitive (i.e. solvent-accessible) surface. That β_T is close to 1 indicates that TS is nearly as compact as the native state; a β_T of 0 indicates a completely disordered and solvent accessible structure, as in the denatured state. As seen in Table 1, all β_T are larger than 0.62 (mean $\beta_T = 0.73 \pm 0.08$ for the two-state variants and 0.76 ± 0.09 for all proteins) and are uniformly distributed along the six-helix bundle. Therefore, the TS exhibits native-like conformation.

In conclusion, we have probed the consequences of mutating topologically conserved packing contacts within the hydrophobic core of the six-helix bundle representing the fusogenic conformation of the SIV gp41 protein. These include both purely non-polar contacts (valine, leucine and isoleucine) and mixed non-polar/polar contacts (glutamine, threonine). There are no obvious (and easily interpretable) trends concerning the role of the probed functions in the hydrophobic core of gp41 in terms of polarity. Also, there is no observed correlation between the size of the mutated non-polar side chain and the resulting thermodynamic and kinetic changes. Thus, the local geometry and any conformational rearrangements compensating the mutation (mostly cavity-creating) dominate the changes in stability and folding/unfolding rates. The presented data demonstrate that some mutations result in large deviations from the apparent two-state behavior that has been postulated for the wild type six-helix bundle [20]. In fact, only two mutants (L10A and I55A) can be strictly classified as two-state folders. This is not completely surprising as in a homotrimeric protein three sites are mutated simultaneously. In the specific case of a coiled coil or a parallel, in-register helical bundle, the mutations are located very close to one another, hence introducing a large packing defect in a particular spot of the hydrophobic core. Nonetheless, nine of the mutants studied which disrupt conserved inter-subunit contacts obey a relaxed two-state criterion. Our quasi-φ-value and quasi-β_T-value analyses lead to the conclusion that the six-helix bundle transverses a compact folding transition state, in which native-like structure formation is modestly advanced, yet there are no completely unstructured regions. Therefore, with all necessary reservations, we propose that the highest-energy barrier along the folding pathway is passed in a trimeric state, after the C-terminal half of each monomer chain is "fixed" in anti-parallel orientation to the surface of the central N-terminal coiled-coil-to-be.

Acknowledgements

This work was supported in part by the Swiss National Science Foundation.

Appendix A. Supplementary data

Supplementary data to this article can be found online at http://dx.doi.org/10.1016/j.bpc.2012.10.004.

References

[1] A. Trkola, T. Dragic, J. Arthos, J.M. Binley, W.C. Olson, G.P. Allaway, C. ChengMayer, J. Robinson, P.J. Maddon, J.P. Moore, CD4-dependent, antibody-sensitive interactions between HIV-1 and its co-receptor CCR-5, Nature 384 (6605) (1996) 184–187.
[2] D.C. Chan, P.S. Kim, HIV entry and its inhibition, Cell 93 (5) (1998) 681–684.
[3] P.A. Bullough, F.M. Hughson, J.J. Skehel, D.C. Wiley, Structure of influenza hemagglutinin at the Ph of membrane-fusion, Nature 371 (6492) (1994) 37–43.
[4] C.M. Carr, C. Chaudhry, P.S. Kim, Influenza hemagglutinin is spring-loaded by a metastable native conformation, Proceedings of the National Academy of Sciences of the United States of America 94 (26) (1997) 14306–14313.
[5] D.L. LeDuc, Y.K. Shin, Insights into a structure-based mechanism of viral membrane fusion, Bioscience Reports 20 (6) (2000) 557–570.
[6] P. Chambers, C.R. Pringle, A.J. Easton, Heptad repeat sequences are located adjacent to hydrophobic regions in several types of virus fusion glycoproteins, Journal of General Virology 71 (1990) 3075–3080.
[7] E.L. Delwart, G. Mosialos, T. Gilmore, Retroviral envelope glycoproteins contain a leucine zipper-like repeat, AIDS Research and Human Retroviruses 6 (6) (1990) 703–706.
[8] R.A. Furuta, C.T. Wild, Y.K. Weng, C.D. Weiss, Capture of an early fusion-active conformation of HIV-1 gp41, Nature Structural Biology 5 (4) (1998) 276–279.
[9] P.L.S. Jones, T. Korte, R. Blumenthal, Conformational changes in cell surface HIV-1 envelope glycoproteins are triggered by cooperation between cell surface CD4 and co-receptors, Journal of Biological Chemistry 273 (1) (1998) 404–409.
[10] I. Munoz-Barroso, S. Durell, K. Sakaguchi, E. Appella, R. Blumenthal, Dilation of the human immunodeficiency virus-1 envelope glycoprotein fusion pore revealed by the inhibitory action of a synthetic peptide from gp41, The Journal of Cell Biology 140 (2) (1998) 315–323.
[11] F.M. Hughson, Enveloped viruses: a common mode of membrane fusion? Current Biology 7 (9) (1997) R565–R569.
[12] J.W. Dubay, S.J. Roberts, B. Brody, E. Hunter, Mutations in the leucine zipper of the human-immunodeficiency-virus type-1 transmembrane glycoprotein affect fusion and infectivity, Journal of Virology 66 (8) (1992) 4748–4756.
[13] M. Lu, H. Ji, S. Shen, Subdomain folding and biological activity of the core structure from human immunodeficiency virus type 1 gp41: implications for viral membrane fusion, Journal of Virology 73 (5) (1999) 4433–4438.
[14] S.C. Blacklow, M. Lu, P. Kim, Trimeric subdomain of the simian immunodeficiency virus glycoprotein, Biochemistry 34 (46) (1995) 14955–14962.
[15] M. Lu, S.C. Blacklow, P.S. Kim, A trimeric structural domain of the HIV-1 transmembrane glycoprotein, Nature Structural Biology 2 (12) (1995) 1075–1082.
[16] M. Caffrey, M. Cai, J. Kaufman, S.J. Stahl, P.T. Wingfield, D.G. Covell, A.M. Gronenborn, G.M. Clore, Three-dimensional solution structure of the 44 kDa ectodomain of SIV gp41, EMBO Journal 17 (16) (1998) 4572–4584.
[17] V.N. Malashkevich, D.C. Chan, C.T. Chutkowski, P.S. Kim, Crystal structure of the simian immunodeficiency virus (SIV) gp41 core: conserved helical interactions underlie the broad inhibitory activity of gp41 peptides, Proceedings of the National Academy of Sciences of the United States of America 95 (16) (1998) 9134–9139.
[18] W. Weissenhorn, A. Dessen, S.C. Harrison, J.J. Skehel, D.C. Wiley, Atomic structure of the ectodomain from HIV-1 gp41, Nature 387 (6631) (1997) 426–430.
[19] D.C. Chan, D. Fass, J.M. Berger, P.S. Kim, Core structure of gp41 from the HIV envelope glycoprotein, Cell 89 (2) (1997) 263–273.
[20] I. Jelesarov, M. Lu, Thermodynamics of trimer-of-hairpins formation by the SIV gp41 envelope protein, Journal of Molecular Biology 307 (2) (2001) 637–656.
[21] D.N. Marti, S. Bjelić, M. Lu, H.R. Bosshard, I. Jelesarov, Fast folding of the HIV-1 and SIV gp41 six-helix bundles, Journal of Molecular Biology 336 (1) (Feb. 2004) 1–8.
[22] J. Liu, S.L. Wang, J.A. Hoxie, C.C. LaBranche, M. Lu, Mutations that destabilize the gp41 core are determinants for stabilizing the simian immunodeficiency virus-CPmac envelope glycoprotein complex, Journal of Biological Chemistry 277 (15) (2002) 12891–12900.
[23] H. Edelhoch, Spectroscopic determination of tryptophan and tyrosine in proteins, Biochemistry 6 (7) (Jul. 1967) 1948–1954.
[24] M.L. Johnson, J.J. Correia, D.A. Yphantis, H.R. Halvorson, Analysis of data from the analytical ultra-centrifuge by non-linear least-squares techniques, Biophysical Journal 36 (3) (1981) 575–588.
[25] T. Laue, B. Shah, S. Pelletier, Computer-aided interpretation of analytical sedimentation data for proteins, in: S. Harding, J. Horton (Eds.), Analytical Ultracentrifugation in Biochemistry and Polymer Science, The Royal Society of Chemistry, Cambridge, 1992.

[26] L. Gonzalez, R.A. Brown, D. Richardson, T. Alber, Crystal structures of a single coiled-coil peptide in two oligomeric states reveal the basis for structural polymorphism, Nature Structural Biology 3 (12) (1996) 1002–1010.
[27] P.B. Harbury, T. Zhang, P.S. Kim, T. Alber, A Switch between 2-stranded, 3-stranded and 4-stranded coiled coils in Gcn4 leucine-zipper mutants, Science 262 (5138) (1993) 1401–1407.
[28] S. Guthe, L. Kapinos, A. Moglich, S. Meier, S. Grzesiek, T. Kiefhaber, Very fast folding and association of a trimerization domain from bacteriophage T4 fibritin, Journal of Molecular Biology 337 (4) (2004) 905–915.
[29] C.D. Geierhaas, A.A. Nickson, K. Lindorff-Larsen, J. Clarke, M. Vendruscolo, BPPred: a Web-based computational tool for predicting biophysical parameters of proteins, Protein Science 16 (1) (2007) 125–134.
[30] I. Jelesarov, H.R. Bosshard, Thermodynamic characterization of the coupled folding and association of heterodimeric coiled coils (Leucine tippers), Journal of Molecular Biology 263 (2) (1996) 344–358.
[31] N.E. Zhou, C.M. Kay, R.S. Hodges, Synthetic model proteins — positional effects of interchain hydrophobic interactions on stability of 2-stranded alpha-helical coiled-coils, Journal of Biological Chemistry 267 (4) (1992) 2664–2670.
[32] A.R. Fersht, Structure and Mechanism in Protein Science, in: W. H. Freeman and company, New York, 1998, pp. 573–614.
[33] S. Bjelić, "Diploma thesis," University of Zurich, 2004.
[34] A.R. Fersht, S. Sato, Phi-value analysis and the nature of protein-folding transition states, Proceedings of the National Academy of Sciences of the United States of America 101 (21) (2004) 7976–7981.
[35] D.P. Raleigh, K.W. Plaxco, The protein folding transition state: what are phi-values really telling us? Protein and Peptide Letters 12 (2) (2005) 117–122.
[36] A. Zarrine-Afsar, A.R. Davidson, The analysis of protein folding kinetic data produced in protein engineering experiments, Methods 34 (1) (2004) 41–50.
[37] A. Zarrine-Afsar, S.L. Lin, P. Neudecker, Mutational investigation of protein folding transition states by Φ-value analysis and beyond: lessons from SH3 domain folding. This paper is one of a selection of papers published in this special issue entitled "Canadian Society of Biochemistry, Molecular &, Biochemistry and Cell Biology 88 (2) (Apr. 2010) 231–238.
[38] M.G. Mateu, M.M.S. Del Pino, A.R. Fersht, Mechanism of folding and assembly of a small tetrameric protein domain from tumor suppressor p53, Nature Structural Biology 6 (2) (1999) 191–198.
[39] L.B. Moran, J.P. Schneider, A. Kentsis, G.A. Reddy, T.R. Sosnick, Transition state heterogeneity in GCN4 coiled coil folding studied by using multisite mutations and crosslinking, Proceedings of the National Academy of Sciences of the United States of America 96 (19) (1999) 10699–10704.
[40] A.R. Fersht, Characterizing transition states in protein folding: an essential step in the puzzle, Current Opinion in Structural Biology 5 (1) (Feb. 1995) 79–84.